Main Manuscript for

Robust longitudinally-variable responses of the ITCZ to a myriad of climate forcings

Alyssa R. Atwood[1], Aaron Donohoe[2], David S. Battisti[3], Xiaojuan Liu[3], Francesco S.R. Pausata[4]

[1]Department of Earth Ocean and Atmospheric Science, Florida State University, Tallahassee, FL, USA; [2]Polar Science Center, Applied Physics Laboratory, University of Washington, Seattle, Washington 98195, USA; [3]Department of Atmospheric Sciences, University of Washington, Seattle, WA 98195, USA; [4]Centre ESCER (Étude et la Simulation du Climat à l'Échelle Régionale) and GEOTOP (Research Center on the dynamics of the Earth System), Department of Earth and Atmospheric Sciences, University of Quebec in Montreal, Montreal, QC, Canada

*Alyssa R. Atwood

Email: aatwood@fsu.edu

ORCiD: 0000-0001-6615-6540

Key Points

- All forcings produce robust regional rainbelt shifts that are larger than (and sometime oppose the direction of) the zonal mean shift
- The central and eastern Pacific provide the greatest contribution to the zonal mean shift and are largely decoupled from the western Pacific
- The direction of the regional shifts under CO_2 forcing is robust across models despite no consensus on the direction of the zonal mean shift

Author Contributions

A.R.A, D.S.B., and A.D. designed the project. A.R.A and A.D. analyzed the modeling simulations, which were conducted by A.R.A. and F.S.R.P. (in addition to the CMIP3 and CMIP5 model simulations that were analyzed), A.R.A wrote the manuscript with contributions from other authors. All authors discussed the results and implications and commented on the manuscript at all stages.

This PDF file includes:

Main Text
Figures 1 to 2

Abstract

We evaluate the longitudinal variation in meridional shifts of the tropical rainbelt in response to natural and anthropogenic forcings using a large suite of coupled climate model simulations. We find that the energetic framework of the zonal mean Hadley cell is generally not useful for characterizing shifts of the rainbelt at regional scales, regardless of the characteristics of the forcing. Forcings with large hemispheric asymmetry such as extratropical volcanic forcing and meltwater forcing give rise to robust zonal mean shifts of the rainbelt, however the direction and magnitude of the shift varies strongly as a function of longitude. Even the Pacific rainband doesn't shift uniformly under any forcing considered. Forcings with weak hemispheric asymmetry such as CO_2 and mid-Holocene forcing give rise to zonal mean shifts that are small or absent, but the rainbelt does shift regionally in coherent ways across models that may have important dynamical consequences.

Plain Language Summary

A band of heavy precipitation spanning the deep tropics is an essential feature of the climate system that diverse ecosystems and billions of people depend on. It is well known that this rainbelt, when averaged across all longitudes, shifts north and south in response to heating or cooling the atmosphere in one hemisphere more than the other; this framework has been widely applied to past tropical rainfall changes under differing climate states. However, we show using many different climate model experiments that this framework does not apply to regional shifts in the rainbelt. Shifts of the rainbelt vary from place to place and thus data documenting north or south shifts in the rainbelt in one location can't be used to infer similar shifts at other longitudes.

Keywords

ITCZ, tropics, rainfall, zonal asymmetry, climate models

Introduction

A large body of literature has emerged over the past two decades demonstrating that there is a latitudinal shift in the distribution of zonally-averaged tropical precipitation in response to hemispheric asymmetry in atmospheric heating that is well constrained by energetic arguments (e.g. 1, 2-5). This relationship arises because both precipitation and atmospheric energy transport in the tropics are largely controlled by the Hadley circulation: precipitation occurs in the ascending branch of the Hadley cell, and the cross-equatorial energy transport is proportional to the strength of the Hadley cell at the equator, which is nearly proportional to the distance of the ascending branch from the equator (6). This energetic framework of the zonal mean Hadley cell provides a useful way to relate changes in the tropical climate to the hemispheric-scale energy budget, and thus shifts in the zonal mean precipitation in idealized and comprehensive model simulations of past, modern, and future climates have been understood in terms of the response to hemispheric asymmetries in atmospheric heating (1-3, 7, 8).

However, while the energetic framework of the zonal mean Hadley cell has been widely used to assess mechanisms of change in the tropical rainbelt on seasonal to orbital timescales, it obscures the inherently regional nature of tropical rainfall. By construction, it averages out the rich zonal variations of tropical rainfall patterns that reflect the distinct processes that govern the large-scale circulation and precipitation in different regions of the tropics. In particular, the dynamics that govern precipitation in monsoon systems are largely distinct from those that govern precipitation in regions of the ocean characterized by strong sea surface temperature gradients and narrow rainbands (i.e. the Intertropical Convergence Zones (ITCZs); e.g. 9, 10). Shifts in tropical precipitation that occur under interhemispheric changes in atmospheric heating thus tend to be zonally-variable and the heat transport changes have been shown to be of limited utility in explaining local rainfall changes (11-14).

Evidence for meridional shifts in tropical rainfall have been found for a variety of past climate states based on proxy records from the tropics and the high latitudes, such as the Last Glacial Maximum (LGM, ~21 kya) when southward shifts of the terrestrial and marine tropical rainbands of up to 7° latitude have been proposed (15, 16), and the North Atlantic iceberg discharge (Heinrich) events of the last glacial period (17-20). A northward shift of the Pacific and Atlantic rainbands of similar magnitude has been proposed during the early-Holocene, when boreal summer insolation was more intense (18-21). During the Little Ice Age (LIA, 1400-1850 CE), a southward shift of the rainbands (by up to 5° latitude) has been inferred from proxy records in and around the tropical Pacific and Atlantic (21-24). Many such paleoclimate studies have invoked the relationship between the zonal mean position of the ITCZ and the cross-equatorial energy flux (and/or interhemispheric temperature gradient) in interpreting meridional shifts of tropical rainfall. However, it is not clear to what degree proxy data documenting regional shifts in rainfall can be extrapolated to infer similar shifts at other longitudes. In many cases, the large regional shifts proposed from paleoclimate records must be regionally localized (as opposed to zonally homogenous) because the cross-equatorial atmospheric heat transport implied from zonal mean ITCZ shifts of that magnitude is physically untenable (25).

In this study, we evaluate the zonal structure of meridional shifts in tropical rainfall in a compilation of climate models under a range of past and future climate forcings. Some forcings are characterized by strong hemispheric asymmetry (e.g. meltwater forcing in the North Atlantic Ocean, extratropical volcanic eruptions, and LGM orography and albedo), while others are characterized by weak hemispheric asymmetry (e.g. quadrupling of CO_2 and mid-Holocene orbital and greenhouse gas forcing). We show that the zonal mean meridional shift of the tropical rainbelt is greater under some forcings than others, but all forcings produce robust regional meridional shifts that are much greater than (and not always in the same direction as) the zonal mean shift.

2. Materials and Methods

2.1. Model simulations

Details of the all the model simulations used in this study are summarized in Table S1. For the response associated with LGM and mid-Holocene forcing, we analyzed model simulations from the Paleoclimate Modeling Intercomparison Project phase 2 (PMIP2)/Coupled modeling Intercomparison project phase 3 (CMIP3) and PMIP3/CMIP5 archives. For the LGM forcing simulations, the forced

response was calculated by averaging years 31-200 after the spin up-period and comparing to the PI control runs. For the mid-Holocene forcing, the forced response was calculated by averaging years 100-685 after the spin up-period and comparing to the PI control runs. For the response to CO_2 forcing, we analyzed simulations from the CMIP5 4×CO2 simulations. The forced response was taken to be the difference between the last 50 years of these simulations and the preindustrial (PI) control simulations.

Response to volcanic forcing is assessed from selected PMIP3 last millennium transient simulations (CCSM4 and GISS Model E ensemble members 122, 125, and 128), CESM Last Millennium Ensemble (LME) volcanic-only simulations, and an ensemble of simulations with Norwegian Earth System Model version 1-M (NorESM) mimicking a high latitude Northern Hemisphere summer eruption (the Laki eruption in Iceland; 26, 27). CCSM4 and CESM LME prescribed sulfate loading (in Tg) from Gao, Robock and Ammann (28) (29) (GRA), while GISS 122, GISS 125, and GISS 128 prescribed volcanic aerosols as functions of AOD and aerosol effective radius with twice the forcing of Crowley, *et al*. (30) (CEA). Years with large extratropical volcanic events (defined as globally averaged AOD > 0.1 and at least 25% greater in one hemisphere), centered around the peak of the event, were compared to the five years prior to the onset of the event and organized into NH and SH composites. In each of the CMIP5 LM and CESM LME simulations, the NH composite consisted of 20 volcanic events and the SH composite consisted of five volcanic events that met these criteria. In the NorESM simulations, the Laki eruption was simulated by adding 100 Tg of SO_2 and dust (as an analog for ash) into the upper troposphere and lower stratosphere over a 4-month period. 48 ensemble members were averaged into three composites (each composite therefore consisting of 16 NH eruptions) in order to be consistent with the CMIP5 LM and CESM LME composites. The NorESM volcanic forcing runs are compared against their own "No Volcano" control run that was branched from the same initial conditions of a transient historical simulation.

For the North Atlantic meltwater forcing simulations, an ensemble of simulations with the Community Earth System Model version 1.0 (CESM 1.0) were used (31). To simulate the atmospheric response to meltwater-induced terminations of the Atlantic overturning circulation, a set of simulations were branched from the control run with 1 Sv of freshwater forcing imposed across the surface of the northern North Atlantic Ocean (50°-70°N) for 100 years. Four ensemble members were performed with this default configuration of CESM by branching from the end of the control run at 9-year intervals. Because it takes 20 years to shut down the AMOC, the last 80 years of these simulations are averaged to create the forced climatology.

Additionally, because the default CESM fully coupled control run is known to have large biases in the mean state of the tropical Pacific compared to observations (Figs. S1, S2; 32) we also apply the same freshwater forcing to a bias corrected version of the model. The mean state bias corrections include both a modification to the topography of central America and surface heat flux modifications, so-called Q-fluxes (also see 33). We raised the height of the mountains in Central America to 1500 m (from 7-18°N, 120-76°W) to reduce the low-level wind biases in the eastern Pacific associated with the poor resolution of Central American topography. Along with the surface heat flux corrections, reductions of these low-level wind biases reduce the tropical sea surface temperature (SST) biases throughout the tropics. In one configuration of the model with three ensemble members we only raised the topography over Central America with no changes in the surface heat fluxes. In a second configuration of the model with four ensemble members we both raise the topography and prescribe a surface heat flux correction with a cyclostationary seasonal cycle throughout the tropical oceans (30°S-30°N) to further reduce the bias in the climatological seasonal cycle in SST. The mean state bias corrections are described in Atwood (31) and in the Supplemental Material. The tropical surface temperature, precipitation, and wind fields before and after these bias corrections are shown in Figs. S1 and S2. The anomalies due to forcing are calculated to be the difference between the final 80 years of each 100 year-long hosing simulations and 100 years of unforced control runs with the same model configuration. We also included two hosing simulations with PMIP2-era models (MPI and HadCM3) in our analyses.

2.2. Changes in the tropical precipitation centroid

Meridional shifts in tropical rainfall are characterized in terms of the mean annual tropical precipitation centroid, P_C (the latitude at which the mean annual area-weighted tropical rainfall to the north equals that to the south, within the bounds 20°N to 20°S). P_C is calculated at each longitude. We

decompose forced changes in P_C (ΔP_C; defined as the difference between a forced simulation and a control simulation) in the following way:

$$\Delta P_C = [\Delta P_C] + \Delta P_C{}^* \quad , \qquad (1)$$

where $[\Delta P_C]$ is the zonal mean change (i.e. ΔP_C averaged over all longitudes) and $\Delta P_C{}^*$ denotes the deviation from the zonal mean. For each set of forcings, in Fig. 1 we compare the change in the zonal mean precipitation centroid $[\Delta P_C]$ to the change in the zonal variation of $\Delta P_C{}^*$ (i.e. the 'waviness' of ΔP_C), quantifying the latter by the standard deviation of ΔP_C across longitudes:

$$\sigma_{Pc} = \left(\frac{1}{N-1}\sum_{j=1}^{N}(\Delta P_C - [\Delta P_C])^2\right)^{1/2} = \left(\frac{1}{N-1}\sum_{j=1}^{N}(\Delta P_C{}^*)^2\right)^{1/2} , \qquad (2)$$

where j = all longitudes. To evaluate the robustness of regional shifts in the precipitation centroid across models, changes in P_C were discretized into zonal bins of width 15º longitude.

3. Results and Discussion

3.1. How does the zonal mean shift of the rainbelt compare to the zonal variations?

The zonal mean shift of the tropical rainbelt is robust across models under climate forcings with strong hemispheric asymmetry. The zonal mean rainbelt shifts south under North Atlantic meltwater forcing, Northern Hemisphere (NH) extratropical volcanic eruptions, and in the majority of models (12/13) under LGM boundary conditions (ordinate of Fig. 1a, d, g; Table 1a). These shifts are expected due to the hemispheric asymmetry in atmospheric heating associated with the slowdown of the Atlantic thermohaline circulation and Arctic sea ice growth in the case of North Atlantic meltwater forcing, the scattering of solar radiation in the NH by stratospheric sulfate aerosols in the case of NH volcanic eruptions, and the presence of large, high albedo NH ice sheets in the case of the LGM. Similarly, the zonal mean rainbelt shifts robustly north under Southern Hemisphere (SH) extratropical volcanic eruptions and weakly north in most models (8/10) under mid-Holocene boundary conditions (Fig. 1i). Only under CO_2 forcing is there no robust ensemble mean shift of the zonal mean rainbelt (Fig. 1k).

There are strong longitudinal variations in ΔP_C under all forcings considered, including those that give rise to large zonal mean shifts of the rainbelt and those that do not. To quantify the zonal mean shift of the rainbelt ($[\Delta P_C]$) relative to its zonal variations (σ_{Pc}) in each set of simulations, the amplitude of the zonal mean change in the tropical precipitation centroid ($[\Delta P_C]$) is compared to the standard deviation of ΔP_C across longitudes (left panels in Fig. 1). In this plane of P_C changes, the blue shaded sector indicates tropical precipitation changes that are more zonally inhomogeneous than they are zonally homogeneous whereas regions in white represent tropical precipitation changes that are more zonally homogenous. Under no forcing is the zonal mean shift substantially larger than the zonal variation (1σ) in the shift, as indicated by the changes in ΔP_C falling near or within the blue shaded sector. Of all the forcings considered, shifts in the mean position of the rainbelt are largest (up to 3.3° latitude) when there is a sufficiently large North Atlantic meltwater forcing to cause a collapse in the Atlantic Meridional Overturning Circulation (Fig. 1a). However, even under this extreme scenario, the zonal variation (1σ) in the shift is as large as the zonal mean shift. Notably, the zonal mean shift and zonal variations are much larger in the CESM simulations without any bias corrections (c.f. simulations 1-4 versus 12-15 in Fig. 1A). A similar relationship between the zonal mean shift and the zonal variations are seen in the rainfall response to extratropical volcanic forcing: although the amplitude of the response is far more muted, the zonal variation in the shift is also of similar magnitude to the zonal mean shift (Fig. 1d).

In contrast to the meltwater and volcanic forcing simulations, under all other forcings considered, the zonal variations in ΔP_C are generally much larger than the zonal mean change in P_C. In the LGM simulations, the zonal variations in ΔP_C range from 0.7 to 3.2° latitude, with some models demonstrating as much zonal variation in ΔP_C as that found in the North Atlantic meltwater simulations ($1.4 \leq \sigma_{Pc} \leq 3.3°$

latitude; Fig. 1a, g). However, the zonal mean shift in the LGM is much smaller than that in response to meltwater forcing (multi-model mean $[\Delta P_C]$ = -0.5° latitude; c.f. ordinate values in Fig. 1a versus 1g). There is general agreement in the sign of the zonal mean shift in the LGM simulations: in 5/7 of the PMIP2 models and all of the PMIP3 models, the zonal mean ITCZ shifts southward by up to 1.4° latitude. The PMIP3 LGM simulations demonstrate a greater zonal mean shift and less zonal variation on average as compared to their PMIP2 counterparts (Fig. 1g); the differences between these two classes of models is most pronounced in the tropical Pacific, where several PMIP2 models demonstrate a northward shift of tropical precipitation in parts of the region (Fig. 1h).

Under mid-Holocene conditions, zonal variations in ΔP_C are on average much smaller (multi-model mean σ_{Pc} = 0.8° latitude) than in the LGM simulations (multi-model mean σ_{Pc} = 1.8° latitude; Table 1a). While the zonal mean shift is also small under mid-Holocene forcing ($[\Delta P_C]$ = 0.3° latitude), there is general consistency in the northward direction of the shift (8/10 models). In contrast, under abrupt 4×CO_2 forcing, zonal variations in ΔP_C (multi-model mean σ_{Pc} = 1.6° latitude) are generally as large as under LGM conditions and far exceed the magnitude of the zonal mean ΔP_C in every model (i.e. all points are well within the blue sector in Fig. 1K). Additionally, there is no consistency in the direction of the zonal mean shift under CO_2 forcing (northward in 9/18 models, southward in 9/18 models). However, the rainbelt does shift regionally in coherent ways across models. The robust aspects of the regional variations in the rainbelt shifts and their contribution to the zonal mean shifts are presented in Section 3.2.

3.2. Where are there robust regional shifts of the rainbelt?

Identifying where robust regional variations of the rainbelt occur in response to a given forcing is important for understanding the globally teleconnected response of the climate system to that forcing, as it is the regional rainfall changes in the tropics that dictate tropical and extratropical teleconnection patterns (through latent heating of the atmosphere) and give rise to regional ocean-atmosphere feedbacks such as the Bjerknes feedback (e.g. 34, 35, 36). To assess the robustness of the regional shifts in the precipitation centroid under each type of forcing, we compare the multi-model mean ΔP_C in discretized zonal bins to the standard deviation of ΔP_C around the mean (i.e. $\pm 1\sigma$ across models) in Fig. 2.

Under North Atlantic meltwater forcing, the rainbelt shifts south robustly across models at all longitudes except for the western Pacific and Maritime Continent, although there is substantial longitudinal variation in the magnitude of the shift (Fig. 2a). A large systematic southward shift occurs in the Atlantic and eastern Pacific Oceans (4-6º latitude) and to a lesser degree over the Indian Ocean and Africa (2.5º latitude). Little to no shift of the rainbelt occurs over the western Pacific, while the shift over the Indian Ocean and Africa is most similar to the zonal mean (2.5º latitude). The longitudinal extent and location of the shift varies widely between models, with the largest intermodel variation in ΔP_C occurring in the central Pacific, where the precipitation centroid is particularly sensitive to changes in the distribution of the northern and southern branches of the Pacific ITCZ. In this region, as well as in the eastern Pacific and Atlantic sectors, the response strongly depends on whether or not the model has been flux-corrected to have a more realistic climatology (Fig. 1b; Fig. S1). In particular, the precipitation response is greater in the Atlantic but smaller in the Pacific in the bias-corrected versions of CESM, as compared to their non-bias-corrected counterparts. The precipitation response increases in the Atlantic when the surface heat flux correction is added (which sharpens the Atlantic rainband; Fig. S1b,c), while the precipitation response decreases in the Pacific when central American topography is raised (as the eastern Pacific low level winds become less responsive to changes in the tropical Atlantic). These bias-corrected versions of the meltwater simulations demonstrate the importance of accurately representing the tropical rainfall climatology to the rainfall responses in these regions.

Under volcanic forcing, the longitudinal structure of the precipitation shift is nearly equal and opposite between the NH and SH eruptions. The amplitude of the zonal mean shift is 0.5-1.0º latitude, similar to the regional shifts over the Atlantic and eastern Indian Oceans and parts of the Maritime Continent (Fig. 2c,d). Larger systematic shifts of 1-2º occur in the central Pacific. The shift is generally weaker over land than ocean regions, with the exception of the western Pacific. As with North Atlantic meltwater forcing, the precipitation centroid over the western Pacific is insensitive to volcanic forcing.

Under LGM boundary conditions, 11/13 models demonstrate a southward shift of tropical precipitation in the zonal mean, though the zonal variations are typically much larger than the small zonal

mean shift (0.5º latitude; Fig. 1g), consistent with the findings of Roberts, Valdes and Singarayer (13). The models diverge widely in their regional representation of the rainbelt response (Fig. 1h), with the largest intermodel variations appearing in the central and western Pacific (where ΔP_C varies from 9º north to 15º south across models; Fig. 1h). However, in most models, rainfall shifts south over South America and the East African/western Indian Ocean sector (Fig. 1h; Fig. 2b). It is these regions, as well as a large southward shift in the central Pacific in some models, that drives the southward zonal mean ITCZ shift in the LGM simulations.

In contrast to the North Atlantic meltwater, volcanic, and LGM simulations, the mid-Holocene and $4\times CO_2$ simulations are characterized by weak interhemispheric asymmetry in their forcings. Under mid-Holocene conditions, 8/10 models demonstrate a weak northward shift of zonal mean tropical rainfall (Fig. 1i), though the zonal variations are substantially larger than the small zonal mean shift, which is only 0.3º latitude in the multi-model mean (Fig. 1a; Fig. 2f). In most models, this zonal mean shift is driven by northward shifts of rainfall over the central Pacific and eastern Africa, while a weak southward shift (opposing the zonal mean) typically occurs over the tropical Atlantic (Fig. 2f).

CO_2 forcing gives rise to the largest zonal variations of any forcing considered and no robust zonal mean precipitation shift (Fig. 1k). However, there are robust and opposing regional shifts in tropical precipitation (Fig. 2e). The rainfall distribution robustly shifts southward in the eastern Pacific and shifts northward by a similar magnitude over the Indian Ocean and East Africa. We emphasize that the direction of these regional shifts in the rainbelt are robust across models despite the wildly diverging direction of the zonal mean rainbelt shift. As with most other forcings, the precipitation centroid over the western Pacific and Maritime Continent is insensitive to CO_2 forcing, while shifts in the central Pacific are large but vary widely across models (Fig. 1l).

Considering all forcings in aggregate, the largest shifts of the mean annual tropical precipitation centroid tend to occur in the central/eastern Pacific, where this metric is particularly sensitive to changes in the distribution of the northern and southern branches of the Pacific ITCZ. However, models also tend to differ widely in their rainfall response to forcing over this region. Tropical mean state biases appear to be a major culprit of the disparate rainfall responses in this region (as indicated by bias-corrected versions of the meltwater simulations), thus highlighting an important caveat to interpreting rainfall changes in this region from model simulations with poor representation of tropical rainfall climatology.

It is clear from all of the forcings analyzed in this study that ΔP_C in the central and eastern Pacific is not simply related to ΔP_C in the western Pacific (Fig. 2). As shown in Fig. 1, the Pacific rainband doesn't shift uniformly across all longitudes under any forcing considered, even within a single model. Under forcings with large hemispheric asymmetry, shifts of the central and eastern Pacific rainband tend to be coordinated with shifts of the Atlantic rainband but are largely decoupled from the western Pacific, where the response of the precipitation centroid is weak under any forcing considered (Fig. 2a-f). When robust shifts of the zonal mean rainbelt occur, the central and eastern Pacific provides the greatest contribution to the zonal mean shift, highlighting the importance of capturing this region when attempting to reconstruct the sign of a change in the zonal mean Hadley circulation from the paleoclimate record.

4. Conclusions

We find that meridional shifts of the tropical rainbelt vary strongly in both magnitude and direction as a function of longitude in response to a variety of natural and anthropogenic forcings. Analysis of a large suite of model simulations demonstrates that the zonal mean framework is generally not useful for characterizing shifts at regional scales regardless of the type of forcing. Forcings with large hemispheric asymmetry (including extratropical volcanic eruptions, meltwater forcing in the North Atlantic Ocean, and the LGM) give rise to robust zonal mean shifts of the rainbelt, however the direction and magnitude of the shift varies strongly as a function of longitude. While under forcings with weak hemispheric asymmetry (including CO_2 quadrupling and mid-Holocene insolation and greenhouse gas forcing), zonal mean shifts are small or absent, but large regional shifts can occur that may have important dynamical consequences.

Robust regional shifts in the tropical rainbelt include a large systematic southward shift (4-6º latitude) in the Atlantic and eastern Pacific Oceans under North Atlantic meltwater forcing. Under extratropical volcanic forcing, the regional structure of the precipitation shift is nearly equal and opposite between the NH and SH eruptions and the shift is generally larger over ocean than land. Under LGM boundary conditions, the models diverge widely in their regional representation of the rainbelt response,

but there is general agreement of a southward shift of zonal mean rainfall driven by changes in the central Pacific, South America, and East Africa/western Indian Ocean. In mid-Holocene simulations, the weak northward shift of zonal mean rainfall is driven by rainfall changes in the central Pacific and eastern Africa. While CO_2 forcing gives rise to large zonal variations and no robust zonal mean shift, tropical rainfall robustly shifts southward over the eastern Pacific, while rainfall shifts northward by a similar magnitude over the Indian Ocean and East Africa. CO_2 forcing highlights the limitations of the zonal mean framework wherein the lack of a robust zonal mean shift across models obscures robust regional shifts of opposing direction (e.g. the eastern Pacific and Indian sectors under CO_2 forcing).

Considering all forcings analyzed in this study, it is notable that the tropical Pacific rainband doesn't shift uniformly under any forcing. The rainband location over the western Pacific and Maritime Continent is relatively insensitive to most types of forcing, while meridional shifts of the central and eastern Pacific rainband tend to be coordinated with the Atlantic rainband under forcings with large hemispheric asymmetry. When robust shifts of the zonal mean rainband occur, the central and eastern Pacific provide the greatest contribution to the zonal mean shift, highlighting the importance of capturing this region when attempting to constrain the sign of the zonal mean Hadley cell change based on networks of paleoclimate data. These findings demonstrate the zonal complexity inherent in shifts in the tropical rainbelt and caution against the practice of inferring large-scale (i.e. Pacific basin wide and larger) changes in the tropical rainbelt based on data from a limited spatial domain.

Acknowledgments

The model precipitation data used in this study were uploaded to Figshare and published with doi: 10.6084/m9.figshare.12284282. All CMIP5/PMIP3 and CMIP3/PMIP2 climate model data were downloaded from the Earth System Grid Federation (ESGF) node hosted by Lawrence Livermore National Laboratory data repositories (https://esgf-node.llnl.gov/). The authors gratefully acknowledge all those who made the CMIP5/PMIP3 and CMIP3/PMIP2 model data open for public access and the many modeling groups who participated in those projects. The authors thank A. Timmermann for providing data from the MPI and HadCM3 meltwater forcing simulations. This material is based upon work supported by the National Science Foundation Paleo Perspective on Climate Change (P2C2) Grant AGS-1702827 awarded to A.D. and A.R.A. Support was provided to D.S.B. and X.L. by grants from the National Science Foundation (Division of Earth Sciences Continental Dynamics Programs Award 1210920 and Frontiers in Earth System Dynamics Award 1338694). Support was also provided to D.S.B by the Tamaki Foundation. F.S.R.P. acknowledges the financial support from the Natural Sciences and Engineering Research Council of Canada (Grant RGPIN-2018-04981) and the Fonds de recherche du Québec – Nature et technologies (2020-NC-268559). We would like to acknowledge C. M. Bitz for assistance in developing the bias-corrected CESM simulations and the high-performance computing support from Cheyenne (doi:10.5065/D6RX99HX) provided by NCAR's Computational and Information Systems Laboratory, sponsored by the National Science Foundation. The NorESM climate model simulations were performed on resources provided by the Swedish National Infrastructure for Computing at the National Supercomputer Centre.

References

1. J. C. H. Chiang, C. M. Bitz, Influence of high latitude ice cover on the marine Intertropical Convergence Zone. *Clim. Dyn.* **25**, 477-496 (2005).
2. S. M. Kang, I. M. Held, D. M. W. Frierson, M. Zhao, The response of the ITCZ to extratropical thermal forcing: Idealized slab-ocean experiments with a GCM. *J. Clim.* **21**, 3521-3532 (2008).
3. D. M. W. Frierson, Y. T. Hwang, Extratropical Influence on ITCZ Shifts in Slab Ocean Simulations of Global Warming. *J. Clim.* **25**, 720-733 (2012).

4. J. C. H. Chiang, A. R. Friedman, Extratropical Cooling, Interhemispheric Thermal Gradients, and Tropical Climate Change. *Annual Review of Earth and Planetary Sciences* **40**, 383-412 (2012).
5. A. Donohoe, J. Marshall, D. Ferreira, D. McGee, The Relationship between ITCZ Location and Cross-Equatorial Atmospheric Heat Transport: From the Seasonal Cycle to the Last Glacial Maximum. *J. Clim.* **26**, 3597-3618 (2013).
6. R. S. Lindzen, A. Y. Hou, Hadley circulations for zonally averaged heating centered off the equator. *J. Atmos. Sci.* **45**, 2416-2427 (1988).
7. W. S. Broecker, A. E. Putnam, Hydrologic impacts of past shifts of Earth's thermal equator offer insight into those to be produced by fossil fuel CO2. *Proceedings of the National Academy of Sciences* **110**, 16710-16715 (2013).
8. Y. T. Hwang, D. M. W. Frierson, S. M. Kang, Anthropogenic sulfate aerosol and the southward shift of tropical precipitation in the late 20th century. *Geophys. Res. Lett.* **40**, 1-6 (2013).
9. L. E. Back, C. S. Bretherton, Geographic variability in the export of moist static energy and vertical motion profiles in the tropical Pacific. *Geophys. Res. Lett.* **33** (2006).
10. M. Biasutti *et al.*, Global energetics and local physics as drivers of past, present and future monsoons. *Nat. Geosci.* **11**, 392-400 (2018).
11. O. Adam, T. Bischoff, T. Schneider, Seasonal and Interannual Variations of the Energy Flux Equator and ITCZ. Part II: Zonally Varying Shifts of the ITCZ. *J. Clim.* **29**, 7281-7293 (2016).
12. J. S. Singarayer, P. J. Valdes, W. H. G. Roberts, Ocean dominated expansion and contraction of the late Quaternary tropical rainbelt. *Scientific Reports* **7**, 9382 (2017).
13. W. H. G. Roberts, P. J. Valdes, J. S. Singarayer, Can energy fluxes be used to interpret glacial/interglacial precipitation changes in the tropics? *Geophys. Res. Lett.* **44**, 6373-6382 (2017).
14. B. R. Boos, R. L. Korty, Regional energy budget control of the intertropical convergence zone and application to mid-Holocene rainfall. *Nat. Geosci.* **9**, 892-897 (2016).
15. A. Koutavas, J. Lynch-Stieglitz, "Variability of the marine ITCZ over the eastern Pacific during the past 30,000 years: Regional perspective and global context" in The Hadley Circulation: Present Past and Future, R. B. a. H. Diaz, Ed. (Springer, 2005), pp. 347-369.
16. J. A. Arbuszewski, P. B. deMenocal, C. Cleroux, L. Bradtmiller, A. Mix, Meridional shifts of the Atlantic intertropical convergence zone since the Last Glacial Maximum. *Nat. Geosci.* **6**, 959-962 (2013).
17. J. C. Stager, D. B. Ryves, B. M. Chase, F. S. R. Pausata, Catastrophic Drought in the Afro-Asian Monsoon Region During Heinrich Event 1. *Science* **331**, 1299-1302 (2011).
18. A. W. Jacobel, J. F. McManus, R. F. Anderson, G. Winckler, Large deglacial shifts of the Pacific Intertropical Convergence Zone. *Nature Communications* **7** (2016).
19. R. H. Rhodes *et al.*, Enhanced tropical methane production in response to iceberg discharge in the North Atlantic. *Science* **348**, 1016-1019 (2015).
20. Y. J. Wang *et al.*, A high-resolution absolute-dated late Pleistocene monsoon record from Hulu Cave, China. *Science* **294**, 2345-2348 (2001).
21. G. H. Haug, K. A. Hughen, D. M. Sigman, L. C. Peterson, U. Rohl, Southward migration of the intertropical convergence zone through the Holocene. *Science* **293**, 1304-1308 (2001).
22. A. Newton, R. Thunell, L. Stott, Climate and hydrographic variability in the Indo-Pacific Warm Pool during the last millennium. *Geophys. Res. Lett.* **33**, L19710 (2006).
23. J. P. Sachs *et al.*, Southward movement of the Pacific intertropical convergence zone AD 1400-1850. *Nat. Geosci.* **2**, 519-525 (2009).
24. F. A. Lechleitner *et al.*, Tropical rainfall over the last two millennia: evidence for a low-latitude hydrologic seesaw. *Scientific Reports* **7** (2017).
25. D. McGee, A. Donohoe, J. Marshall, D. Ferreira, Changes in ITCZ location and cross-equatorial heat transport at the Last Glacial Maximum, Heinrich Stadial 1, and the mid-Holocene. *Earth Planet. Sci. Lett.* **390**, 69-79 (2014).

26. F. S. R. Pausata, L. Chafik, R. Caballero, D. S. Battisti, Impacts of high-latitude volcanic eruptions on ENSO and AMOC. *Proceedings of the National Academy of Sciences* **112** (2015).
27. F. S. R. Pausata, A. Grini, R. Caballero, A. Hannachi, O. Seland, High-latitude volcanic eruptions in the Norwegian Earth System Model: the effect of different initial conditions and of the ensemble size. *Tellus B: Chemical and Physical Meteorology* **67** (2015).
28. C. Gao, A. Robock, C. Ammann, Volcanic forcing of climate over the past 1500 years: An improved ice core-based index for climate models. *Journal of Geophysical Research-Atmospheres* **113**, D231111 (2008).
29. L. Landrum *et al.*, Last Millennium Climate and Its Variability in CCSM4. *J. Clim.* **26**, 1085-1111 (2013).
30. T. J. Crowley *et al.*, Volcanism and the Little Ice Age. *PAGES Newsletter* **16**, 22-23 (2008).
31. A. R. Atwood (2015) Mechanisms of Tropical Pacific Climate Change During the Holocene." in *PhD thesis* (University of Washington).
32. G. Li, S.-P. Xie, Tropical Biases in CMIP5 Multimodel Ensemble: The Excessive Equatorial Pacific Cold Tongue and Double ITCZ Problems. *J. Clim.* **27**, 1765-1780 (2014).
33. H. Zhang *et al.*, East Asian hydroclimate modulated by the position of the westerlies during Termination I. *Science* **362**, 580-583 (2019).
34. A. E. Gill, Some simple solutions for heat-induced tropical circulation. *Q. J. Roy. Meteorol. Soc.* **106**, 447-462 (1980).
35. J. M. Wallace *et al.*, On the structure and evolution of ENSO-related climate variability in the tropical Pacific: Lessons from TOGA. *J. Geophys. Res.* **103**, 14,241-214,259 (1998).
36. K. E. Trenberth, J. M. Caron, D. P. Stepaniak, S. Worley, Evolution of El Nino-Southern Oscillation and global atmospheric surface temperatures. *Journal of Geophysical Research-Atmospheres* **107** (2002).
37. X.-G. Xin, T.-W. Wu, J. Zhang, Introduction of CMIP5 experiments carried out with the climate system models of Beijing Climate Center *Advances in Climate Change Research* **4**, 41-49 (2013).
38. P. R. Gent *et al.*, The Community Climate System Model Version 4. *J. Clim.* **24**, 4973-4991 (2011).
39. A. Voldoire *et al.*, The CNRM-CM5.1 global climate model: description and basic evaluation. *Clim. Dyn.* **40**, 2091-2121 (2013).
40. L. D. Rotstayn *et al.*, Improved simulation of Australian climate and ENSO-related rainfall variability in a global climate model with an interactive aerosol treatment. *Int. J. Climatol.* **30**, 1067-1088 (2010).
41. L. Li *et al.*, The flexible global ocean-atmosphere-land system model, Grid-point Version 2: FGOALS-g2. *Adv. Atmos. Sci.* **30**, 543-560 (2013).
42. Q. Bao *et al.*, The Flexible Global Ocean-Atmosphere-Land system model, Spectral Version 2: FGOALS-s2. *Adv. Atmos. Sci.* **30**, 561-576 (2013).
43. G. A. Schmidt *et al.*, Present-day atmospheric simulations using GISS ModelE: comparison to in situ, satellite, and reanalysis data. *J. Clim.* **19**, 153-192 (2006).
44. G. A. Schmidt *et al.*, Configuration and assessment of the GISS ModelE2 contributions to the CMIP5 archive. *Journal of Advances in Modeling Earth Systems* **6**, 141-184 (2014).
45. S. Watanabe *et al.*, MIROC-ESM 2010: model description and basic results of CMIP5-20c3m experiments. *Geosci. Model Dev.* **4**, 845-872 (2011).
46. T. J. Raddatz *et al.*, Will the tropical land biosphere dominate the climate–carbon cycle feedback during the twenty-first century? *Clim. Dyn.* **29**, 565-574 (2007).
47. S. J. Marsland, H. Haak, J. H. Jungclaus, M. Latif, F. Röske, The Max-Planck-Institute global ocean/sea ice model with orthogonal curvilinear coordinates. *Ocean Modelling* **5**, 91-127 (2003).

48. S. Yukimoto *et al.*, A New Global Climate Model of the Meteorological Research Institute: MRI-CGCM3 - Model Description and Basic Performance. *Journal of the Meteorological Society of Japan. Ser. II* **90A**, 23-64 (2012).
49. K. E. Taylor, R. J. Stouffer, G. A. Meehl, An overview of CMIP5 and the experiment design. *Bull. Am. Meteorol. Soc.* **93**, 485-498 (2012).
50. T. Iversen *et al.*, The Norwegian Earth System Model, NorESM1-M – Part 2: Climate response and scenario projections. *Geosci. Model Dev.* **6**, 389-415 (2013).
51. S. P. Harrison *et al.*, Climate model benchmarking with glacial and mid-Holocene climates. *Clim. Dyn.* **43**, 671-688 (2014).
52. D. Salas-Melia *et al.*, Description and validation of the CNRM-CM3 global coupled model. *CNRM working note* **103** (2005).
53. Y. Yongqiang, Y. Rucong, Z. Xuehong, L. Hailong, A flexible coupled ocean-atmosphere general circulation model. *Adv. Atmos. Sci.* **19**, 169-190 (2002).
54. C. Gordon *et al.*, The simulation of SST, sea ice extents and ocean heat transports in a version of the Hadley Centre coupled model without flux adjustments. *Clim. Dyn.* **16**, 147-168 (2000).
55. O. Marti *et al.*, The new IPSL climate system model: IPSL-CM4. *Note du Pôle de Modélisation, IPSL* **26**, 1-86 (2005).
56. K-1-Model-Developers (2004) K-1 Coupled GCM (MIROC) Description. in *K-1 technical report 1*, eds H. Hasumi, S. Emori (Center for Climate System Research, University of Tokyo).
57. E. Roeckner *et al.* (2003) The atmospheric general circulation model ECHAM5—Part I: Model description. in *Max-Planck-Institut für Meteorologie, Technical Report*.
58. B. L. Otto-Bliesner *et al.*, Last Glacial Maximum and Holocene Climate in CCSM3. *J. Clim.* **19**, 2526-2544 (2006).
59. C. M. Colose, A. N. LeGrande, M. Vuille, Hemispherically asymmetric volcanic forcing of tropical hydroclimate during the last millennium. *Earth System Dynamics* **7**, 681-696 (2016).
60. B. L. Otto-Bliesner, E. C. Brady, J. Fasullo, Climate Variability and Change since 850 CE: An Ensemble Approach with the Community Earth System Model *Bull. Am. Meteorol. Soc.* **97**, 735-754 (2016).

Figures and Tables

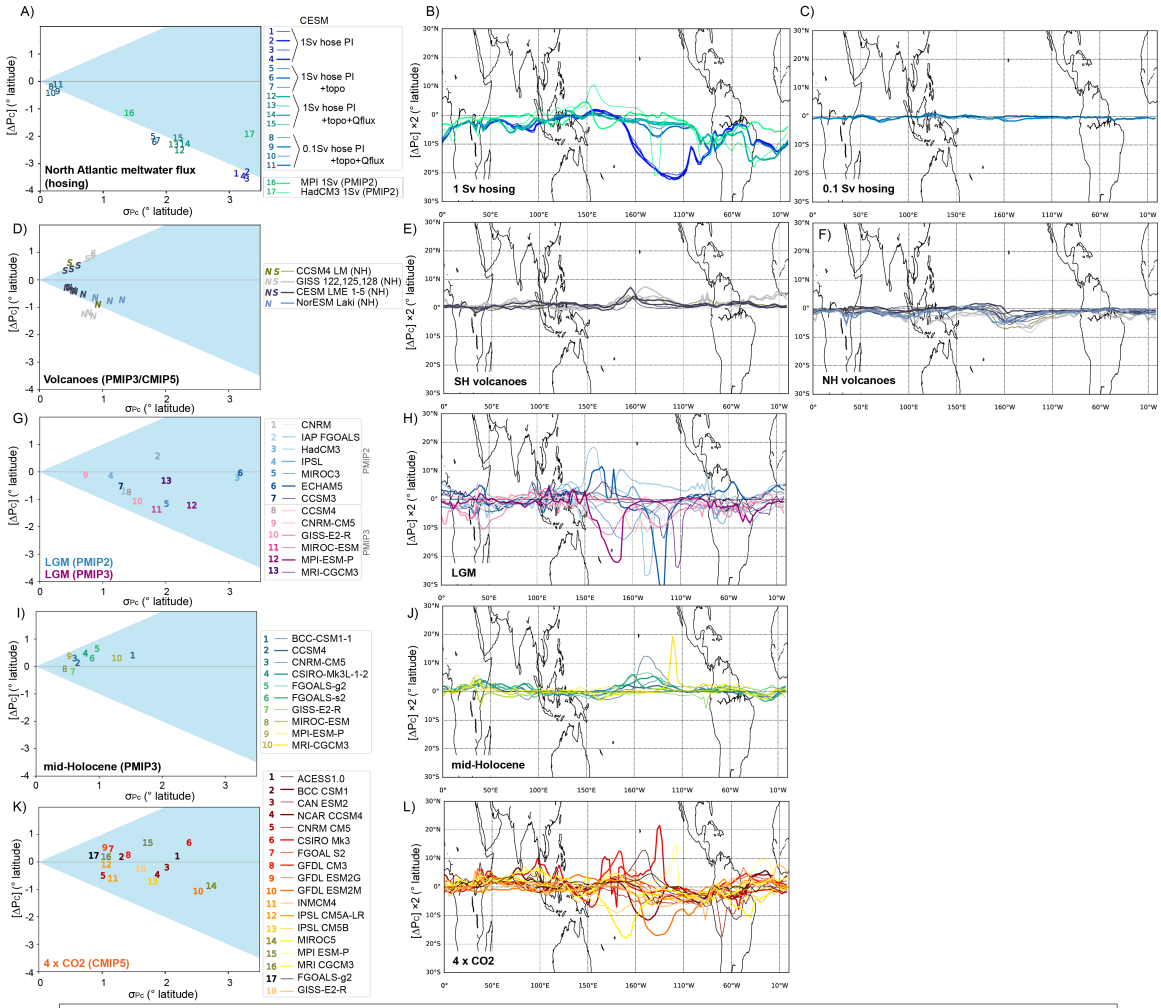

Figure 1. The meridional shift in the tropical precipitation centroid (ΔPc) under different climate forcings and boundary conditions. Left panels: Zonal-mean shift in the precipitation centroid ([ΔPc]) versus the standard deviation of ΔPc* (σ_{Pc}; see Eqns.1-2). The blue triangle indicates the region where the longitudinal variations in ΔPc are as large, or larger than the zonal-mean change in ΔPc. Middle and right panels: 2×ΔPc

as a function of longitude, where the meridional displacement is multiplied by a factor of two for visual clarity.

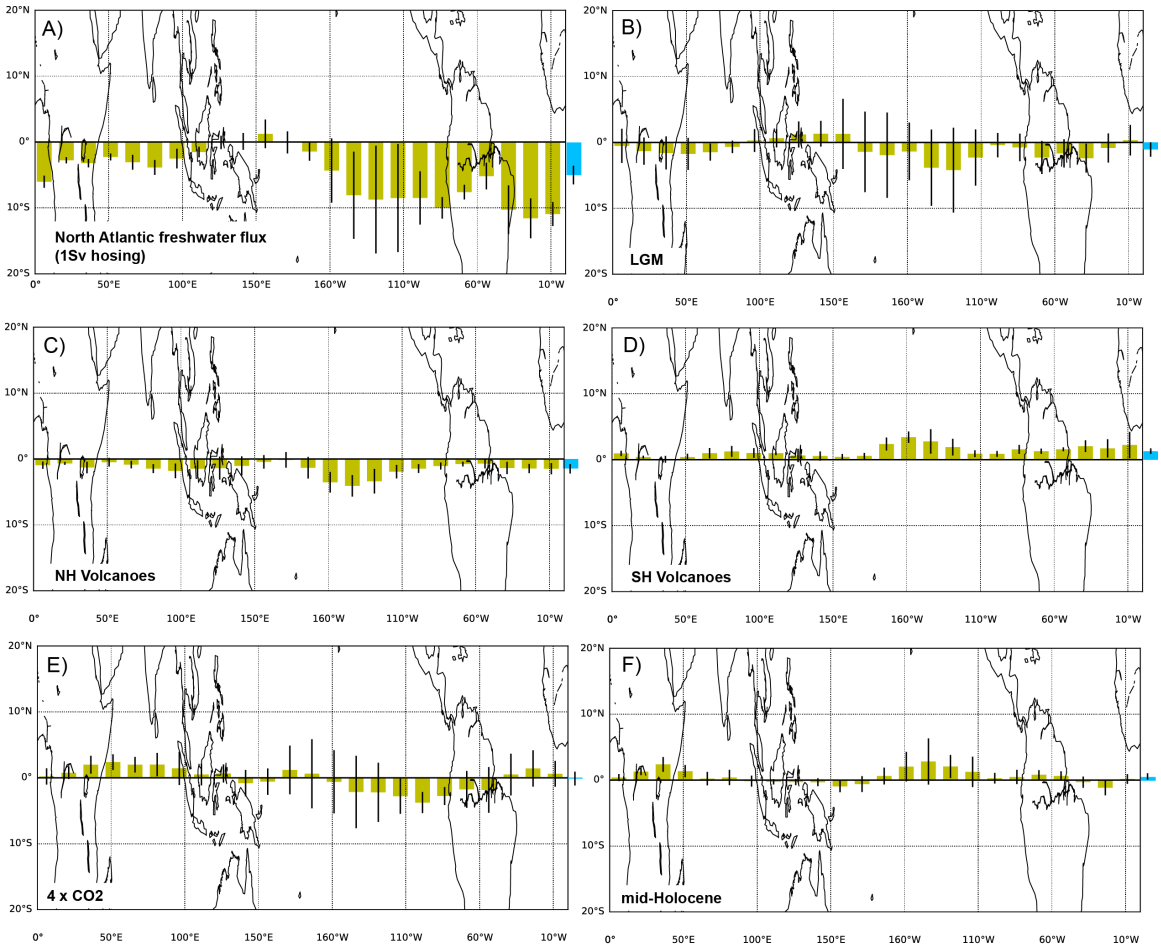

Figure 2. Change in tropical precipitation centroid (ΔPc) as a function of longitude under different climate forcings and boundary conditions. Yellow bars indicate the multi-model mean ΔPc (multiplied by a factor of two for visual clarity) averaged over zonal bins of width 15° longitude. The whiskers represent ± 1σ across models. Blue bars indicate the multi-model mean zonally-averaged ΔPc ([Pc]), also multiplied by a factor of two for visual clarity.

Figure 2. Change in tropical precipitation centroid (ΔPc) as a function of longitude under different climate forcings and boundary conditions. Yellow bars indicate the multi-model mean ΔPc (multiplied by a factor of two for visual clarity) averaged over zonal bins of width 15° longitude. The whiskers represent ± 1σ across models. Blue bars indicate the multi-model mean zonally-averaged ΔPc ([Pc]), also multiplied by a factor of two for visual clarity.